

Seismic metamaterial barriers for ground vibration mitigation in railways considering the train-track-soil dynamic interactions

Li, Ting; Su, Qian; Kaewunruen, Sakdirat

Document Version
Peer reviewed version

Citation for published version (Harvard):

Li, T, Su, Q & Kaewunruen, S 2020, 'Seismic metamaterial barriers for ground vibration mitigation in railways considering the train-track-soil dynamic interactions', *Construction and Building Materials*.

[Link to publication on Research at Birmingham portal](#)

General rights

Unless a licence is specified above, all rights (including copyright and moral rights) in this document are retained by the authors and/or the copyright holders. The express permission of the copyright holder must be obtained for any use of this material other than for purposes permitted by law.

- Users may freely distribute the URL that is used to identify this publication.
- Users may download and/or print one copy of the publication from the University of Birmingham research portal for the purpose of private study or non-commercial research.
- User may use extracts from the document in line with the concept of 'fair dealing' under the Copyright, Designs and Patents Act 1988 (?)
- Users may not further distribute the material nor use it for the purposes of commercial gain.

Where a licence is displayed above, please note the terms and conditions of the licence govern your use of this document.

When citing, please reference the published version.

Take down policy

While the University of Birmingham exercises care and attention in making items available there are rare occasions when an item has been uploaded in error or has been deemed to be commercially or otherwise sensitive.

If you believe that this is the case for this document, please contact UBIRA@lists.bham.ac.uk providing details and we will remove access to the work immediately and investigate.

1 **Seismic metamaterial barriers for ground vibration mitigation in railways**
2 **considering the train-track-soil dynamic interactions**

3 Ting Li^{a,b,c}, Qian Su^{a,b}, Sakdirat Kaewunruen^{c,*}

4 ^a *School of Civil Engineering, Southwest Jiaotong University, Chengdu 610031, China*

5 ^b *Key Laboratory of High-Speed Railway Engineering, Ministry of Education, Southwest Jiaotong*
6 *University, Chengdu 610031, China*

7 ^c *School of Engineering, University of Birmingham, Birmingham B15 2TT, UK*

8 *Correspondence should be addressed to Sakdirat Kaewunruen (s.kaewunruen@bham.ac.uk).

9
10 **Abstract:** With the rapid development of high speed rail system, ground vibration mitigation
11 solutions are desperately needed. Based on the concepts of phononic crystals, seismic
12 metamaterial, which is a novel vibration mitigation method, can **theoretically** yield excellent
13 performance in shielding dynamic propagation waves in broad frequency bands. However, the
14 application of seismic metamaterials in railway-induced vibration mitigation is a recent and
15 ongoing topic. Therefore, this study aims to create new contribution towards a better
16 understanding into the mitigation effects by seismic metamaterials for railway-induced
17 ground vibrations. The seismic metamaterials are made of an array of concrete inclusions in
18 this study. The dispersion theory for seismic metamaterials is proposed for analyzing the
19 theoretical band gaps. A 3D coupled train-track-soil interaction model is also developed based
20 on the multi-body simulation principle, finite element theory, and perfectly matched layers
21 method using LS-DYNA. The dimensions of seismic metamaterials are determined based on
22 the dominant frequencies of vibration accelerations in natural ground. When the seismic
23 metamaterials are adopted in railway ground, the vibration responses are investigated in both
24 time and frequency domains to illustrate the mitigation effects. Finally, the numbers of
25 inclusions, initial distances, and train speeds are changed to investigate their influences on
26 shielding effects. The insight from this study provides a new and better understanding of
27 attenuating ground vibrations using seismic metamaterials in high speed railways.

28 **Keywords:** seismic metamaterials; band gap; ground vibration mitigation; train-track-soil
29 interactions

30 1. Introduction

31 High-speed rail is undergoing rapid development with the demand to increase operating
32 train speeds all over the world [1-3]. Numerous high-speed trains with a maximum operating
33 speed of 380 km/h are traveling in China. The demand to elevate train speed brings new
34 challenges for high-speed rail infrastructures, especially for the ground-borne vibrations.
35 Train-induced ground vibrations can negatively affect surrounding residents, buildings,
36 tunnels, drainage systems, overhead wiring structures, and so on [4, 5, 34, 35, 36]. Effective
37 and efficient vibration mitigation solutions are desperately needed for high speed rail
38 networks.

39 Considerable efforts have been made for the mitigation of the railway-induced vibrations.
40 Active isolation techniques, such as floating slab tracks, softer rail pads and resilient wheels,
41 have been investigated to attenuate railway vibrations from sources [6, 7]. Mitigation
42 measures can also be applied to the propagation paths of dynamic waves in soils, termed as
43 passive isolation. The passive isolation solutions can be open trenches, in-filled trenches,
44 sheet pile walls, and so on [8, 9]. Although these solutions exhibit good vibration attenuation
45 performance, there are some difficulties in practice when these structures are constructed in
46 soils. For instance, the stability of opening holes is a concern, and the trench is challenging to
47 be built in unstable and soft soils [10]. As a type of passive isolation, seismic metamaterial
48 (SMM), which is a recently proposed solution based on the concepts of phononic crystals, is
49 receiving increasing attention [11, 12].

50 The term metamaterials emerged from electromagnetism in a nano-scale world. During
51 the last several decades, the investigation of SMM in attenuating all types of waves, such as
52 ultrasound, acoustic, elastic, electromagnetic waves and even thermal fluctuations, has drawn
53 considerable interest from a large number of scientists and engineers [13-15]. In engineering,
54 SMM is a type of unique material designed and built to acquire one (or more than one)
55 property not found in naturally occurring materials, such as a negative index of refraction [16].
56 The inclusions of SMM are normally designed using a combination of multiple elements
57 arranged in repeating patterns. Due to the periodicity of the structure, the filtering effect of the
58 SMM provides the possibility to attenuate the vibration in certain frequency bands. When the

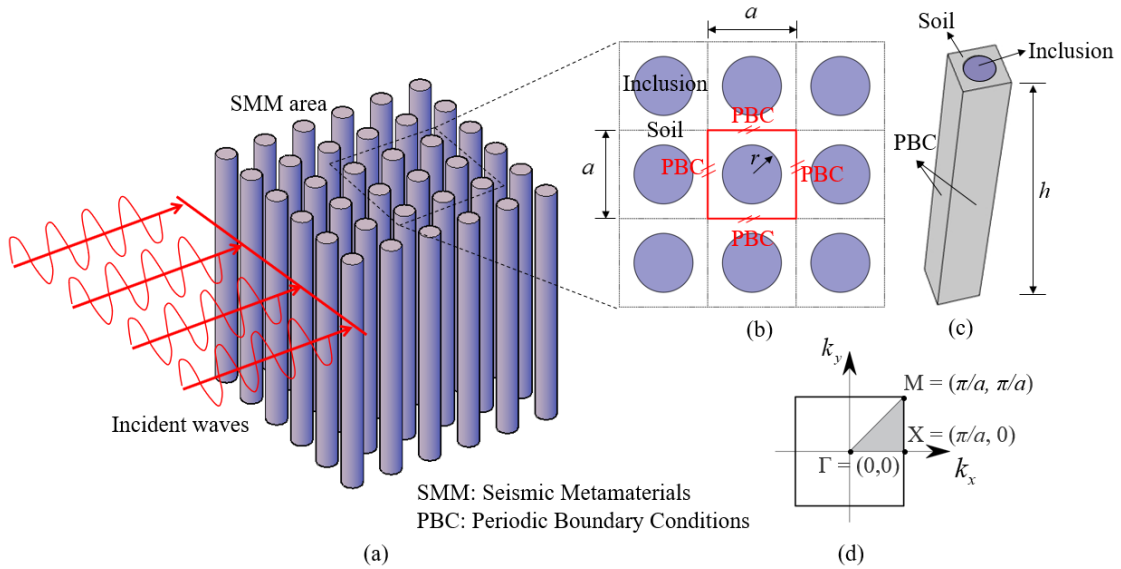
59 frequencies of the incident waves fall into a blind zone, termed as band gap, the waves can be
60 blocked in any directions, so that they cannot propagate anymore [17, 18].

61 With the development of the SMM field, many types of SMM have emerged with a
62 decade of research. Based on the literature review, Brule et al. [14] proposed four categories
63 of the SMM: seismic soil-metamaterials [19, 20], buried mass-resonators [21], above-surface
64 resonators [11, 12], and auxetic materials [22]. The seismic-soil metamaterials are quite
65 convenient to be adopted in soils. Brule et al. [23, 24] designed the SMM with a grid of
66 cylindrical holes in soils and carried out large-scale field tests to investigate the Bragg's effect
67 and distribution of energies in soils. The band gap of such kind of SMM is around 50 Hz.
68 Miniaci et al. [25] investigated the parameters that affect band gaps of SMM by carrying out a
69 numerical analysis with large-scale mechanical metamaterials, which are made of cavities or
70 rubber/steel/concrete-infilled inclusions. Numerous scholars have also investigated the band
71 gaps of SMM by adopting an array of piles, which possess an excellent performance in
72 mitigating vibrations [19, 20, 26]. Despite the recent advances in this field, the SMM is
73 mostly designed for shielding seismic waves from earthquakes. Kaewunruen et al. [16] were
74 the first to evaluate the railway-induced ground vibration mitigation using SMM with the aim
75 of life-cycle performance analysis, indicating that the SMM has a high possibility to be used
76 as wave barriers in railway ground. Thompson et al. [27] also proposed that the application of
77 SMM in attenuating railway-induced ground vibrations is an open question and needs further
78 investigations.

79 Considering the vibration mitigation by SMM is recent, and the related research is still
80 ongoing, this study aims to give a contribution of understanding the mitigation effects of
81 SMM adopted in railways by carrying out a numerical analysis. An array of piles is chosen to
82 be SMM in this study as the pile inclusions are the simplest way to be constructed in practice.
83 The dispersion theory for SMM is first introduced to find out the theoretical band gaps. Then,
84 a 3D coupled train-track-soil interaction model is developed using LS-DYNA to investigate
85 the ground vibration mitigation effects using SMM. This study could bring an insightful and
86 new understanding of the vibration mitigation by the novel solution of SMM in high-speed
87 railways.

88 **2. Dispersion theory for seismic metamaterials**

89 The dispersion characteristics of the seismic metamaterial (SMM) can theoretically
 90 demonstrate the ground vibration mitigation components in frequency domain since the
 91 dispersion relation of the SMM illustrates the modes of wave propagation with passbands and
 92 band gaps, where seismic waves cannot pass. The dispersion theory for SMM is thus firstly
 93 introduced.



94
 95 Figure 1 Schematic representation of the SMM (a) Periodic array of barriers (b) Plan view (c) Unit
 96 cell in Comsol Multiphysics (d) The first Brillouin zone with the irreducible part (light grey
 97 triangle of vertices Γ -X-M)

98 As shown in Figure 1 (a), the SMM appears typically as a periodic array of barriers to
 99 interact with the incident waves to mitigate the vibration responses. The concrete piles with
 100 circular sections are considered as inclusions of the SMM in this study. Both soil and
 101 inclusion are assumed to be homogenous, linearly elastic, and perfectly bonded materials
 102 [20].

103 **2.1 Wave equation**

104 For the isotropic, linear elastic medium without considering of damping and body force,
 105 the governing equation of waves propagating in periodic structures is written as follows [20]:

106
$$\rho \frac{\partial^2 \mathbf{u}}{\partial t^2} - \nabla \cdot c \nabla \mathbf{u} = 0 \quad (1)$$

107 where ρ is the mass density, \mathbf{u} is the displacement vector, t is time, ∇ is differential operator,
 108 and c is the elastic constant.

109 2.2 Floquet-Bloch theory and periodic boundary conditions

110 Since the SMM is a periodic system, a unit cell with the lattice constant a can be
 111 studied for the dispersion relations by applying periodic boundary, as shown in Figure 1 (b)
 112 and (c). The Floquet-Bloch theory was originally developed to solve the differential equations
 113 of wave-like particles in physical sciences, and it is adopted here to study the behavior of
 114 wave propagation in the periodic unit cell [12]. According to the Floquet-Bloch theory, the
 115 displacement vector in Eq. (1) can be written as:

116
$$\mathbf{u}(\mathbf{r}, t) = e^{i(\mathbf{k} \cdot \mathbf{r} - \omega t)} \mathbf{u}_{\mathbf{k}}(\mathbf{r}) \quad (2)$$

117 where \mathbf{k} is the Floquet-Bloch wave vector in the first Brillouin zone [28], \mathbf{r} is the
 118 coordinate vector, ω is the angular frequency, and $\mathbf{u}_{\mathbf{k}}(\mathbf{r})$ is a modulation function of the
 119 displacement vector. The modulation function is a periodic function defined in the unit cell:

120
$$\mathbf{u}_{\mathbf{k}}(\mathbf{r}) = \mathbf{u}_{\mathbf{k}}(\mathbf{r} + \mathbf{a}) \quad (3)$$

121 where \mathbf{a} is the lattice constant vector, $\mathbf{a} = (a_x, a_y)$. In this study, the inclusions are
 122 arranged in the shape of square, therefore $a_x = a_y = a$.

123 Substituting Eq. (3) into Eq. (2), the periodic boundary conditions (PBC) for a unit cell
 124 are obtained,

125
$$\mathbf{u}_{\mathbf{k}}(\mathbf{r} + \mathbf{a}, t) = e^{i\mathbf{k} \cdot \mathbf{a}} \mathbf{u}_{\mathbf{k}}(\mathbf{r}, t) \quad (4)$$

126 2.3 Dispersion equation and solutions

127 By combining the Eq. (1) and Eq. (4), the dispersion relation of a periodic system can be
 128 transferred into an eigenvalue equation:

$$(\mathbf{\Omega}(\mathbf{k}) - \omega^2 \mathbf{M}) \cdot \mathbf{u} = \mathbf{0} \quad (5)$$

129

130 where $\mathbf{\Omega}(\mathbf{k})$ and \mathbf{M} are the stiffness and mass matrices of the unit cell, respectively. The
131 dispersion relation is an implicit function between the wave vector \mathbf{k} and eigenfrequency ω .
132 In order to consider all the wave propagation modes, the wave vector \mathbf{k} should be changed
133 across the boundary of the first irreducible Brillouin zone (Γ -X-M) [28], as shown in Figure 1
134 (d). For a wave vector where no frequency exists, it is termed the band gap, where no wave
135 propagation appears.

136 The commercial software Comsol Multiphysics is used to solve the eigenvalue equation
137 and dispersion relation. It is noted that the soil and inclusion are normally modeled with a
138 large depth h to simulate the infinite thickness of the unit cell [29]. The PBC is applied to all
139 vertical sides of the unit cell, while a fixed boundary is adopted on the bottom surface. The
140 eigenfrequency studies and complex boundaries as Eq. (4) are chosen in the software. The
141 eigenfrequencies are obtained by sweeping wave vectors in the first irreducible Brillouin zone,
142 and the dispersion relation of the SMM is obtained by solving the eigenvalue equation.

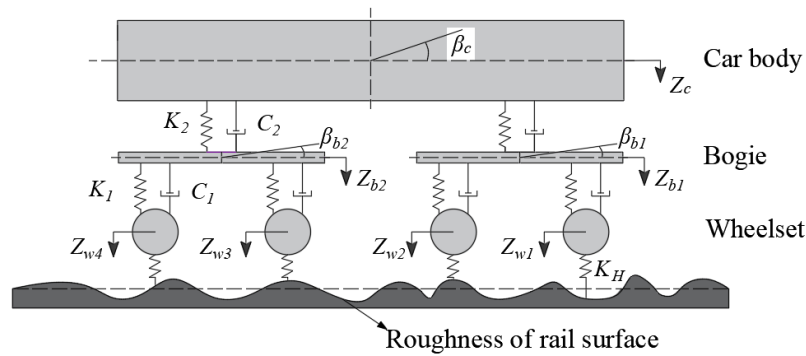
143 3. Modeling of the train-track-soil dynamic interactions

144 Although the dispersion relation of the SMM illustrates the characteristics of seismic
145 wave propagations, there are lots of assumptions with ideal conditions when the theoretical
146 dispersion relation is obtained. The ground vibration mitigation effect using SMM in
147 high-speed railways is unknown in practice. In order to investigate the ground vibration
148 attenuation level using SMM in railways, a novel 3D coupled train-track-soil model is
149 developed in LS-DYNA. The high-speed train is simulated based on the multi-body
150 simulation (MBS) principle, and the slab track is developed based on the finite element
151 modeling (FEM) theory. The soils and the SMM are simulated based on the FEM theory
152 together with the Perfectly Matched Layers (PML) method.

153 3.1 Modeling of the high-speed train and slab track

154 A commonly operated Chinese high-speed train, the China Railway High-speed (CRH)

155 380 Electric Multiple Unit (EMU) train, is simulated in this model. The vehicle consists of
 156 one car body, two bogies, four wheelsets, and two stage-suspension systems, as shown in
 157 Figure 2. The car body, bogies, and wheelsets are simplified as the rigid-bodies using shell
 158 and beam elements. The springs and dashpots connect these multi-rigid-bodies. As the vertical
 159 vibration is the primary excitation to the infrastructures, the vertical degrees of freedom (DOF)
 160 of the vehicle are considered in this model. The vehicle has 10 DOF, including the vertical
 161 and pitch motion of car body (Z_c, β_c), the vertical and pitch motion of bogies
 162 ($Z_{bi}, \beta_{bi} \ i = 1, 2$), and the vertical motion of wheelsets ($Z_{wi} \ i = 1, \dots, 4$).



163
 164 Figure 2 Simulation of the vehicle

165 The China Railway Track System (CRTS) II slab track is adopted in this model. It
 166 consists of rail, rail pads, concrete slab, cement asphalt (CA) mortar layer, and concrete base
 167 [30]. The rail is simulated as the Euler beam, which is supported by the discrete springs and
 168 dashpots to represent the rail pads. This beam model may yield around 5-8% of discrepancy
 169 when compared with Timoshenko beam theory. However, this discrepancy is acceptable for
 170 the purpose of track substructure vibration analysis since the vibrations at lower layers of
 171 tracks are already suppressed by the track structure [2]. The concrete slab, CA mortar, and
 172 concrete base are simulated as solid elements with brick mesh.

173 The contact between wheel and rail is simulated based on the Hertz contact theory by
 174 using keywords: *Rail_Track and *Rail_Train. LS-DYNA can automatically calculate the
 175 wheel-rail contact force based on the following equation:

$$176 \quad F = K_H \times (Z_w - Z_r - \delta) \quad (6)$$

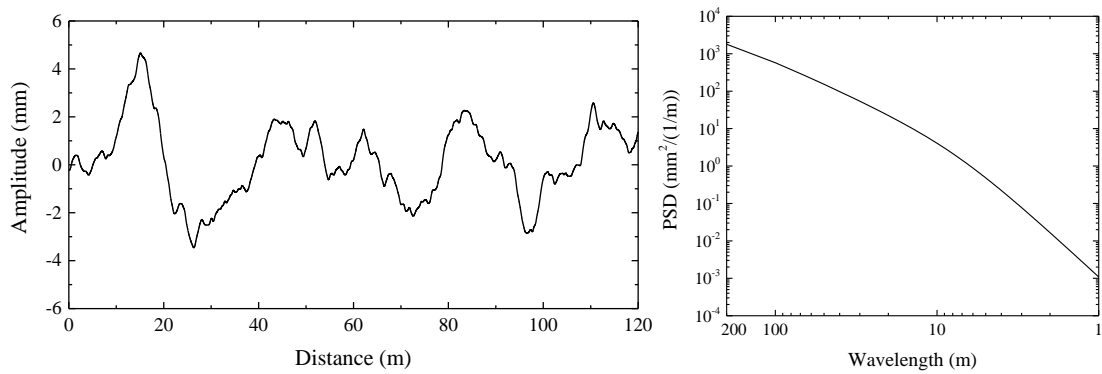
177 where K_H is the vertical stiffness of the wheel-rail contact spring, $K_H = 1.325 \times 10^9$ N/m in
 178 this study [31]; Z_w is the vertical displacement of the wheel; Z_r is the vertical displacement of
 179 the rail; and δ is the roughness of rail surface. The Germany high-speed low disturbance

180 irregularity is used to excite the wheel-rail contact. The power spectrum density (PSD)
 181 function of the roughness is calculated as follows:

$$182 \quad S_v(\Omega) = \frac{A_v \Omega_c^2}{(\Omega^2 + \Omega_r^2)(\Omega^2 + \Omega_c^2)} \quad (7)$$

183 where A_v is the roughness constant ($A_v = 4.032 \times 10^{-7} \text{ m}^2 \cdot \text{Rad/m}$); Ω_c and Ω_r are the cutoff
 184 frequency ($\Omega_c = 0.8246 \text{ rad/m}$, $\Omega_r = 0.0206 \text{ rad/m}$); and Ω is the spatial frequency of the
 185 roughness. The PSD function can be transformed into vertical roughness along the
 186 longitudinal distance of the track using a time-frequency transformation technique, as shown
 187 in Figure 3.

188 The material properties of the CRH380 EMU Train and CRTS II slab track can be found
 189 from [4] and [5].



190

191 (a) Roughness with distance

191 (b) PSD with wavelength

192

Figure 3 The roughness of rail surface

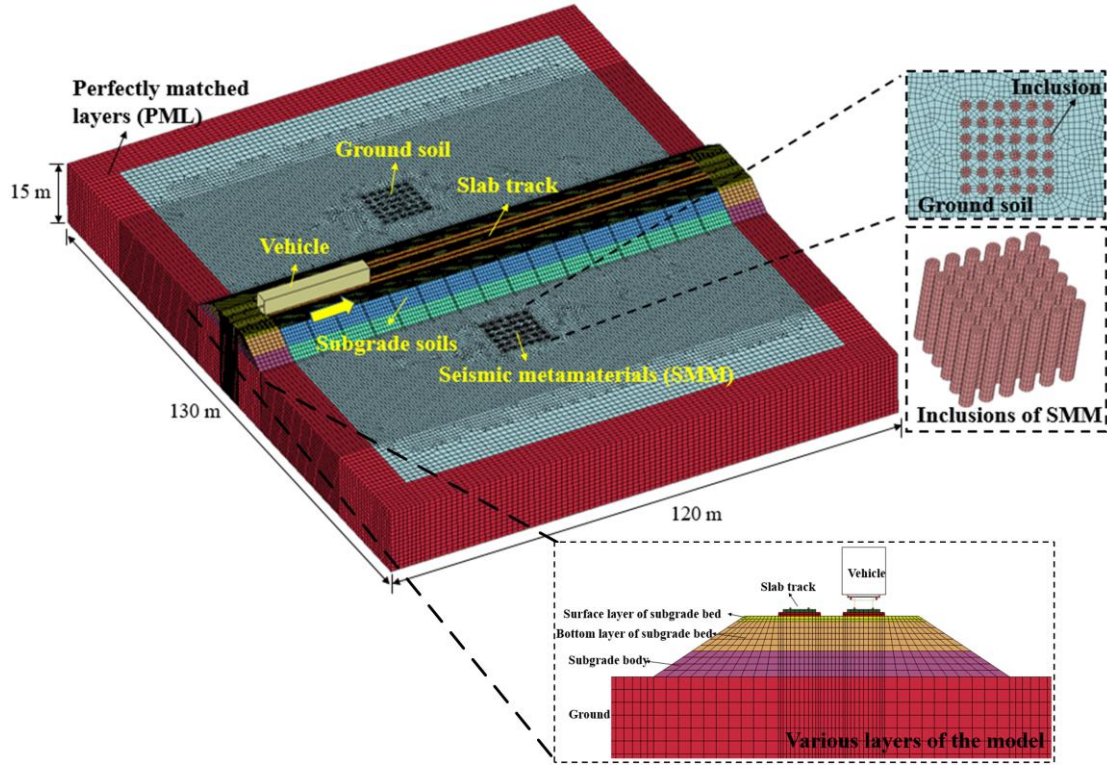
193 3.2 Modeling of soils and seismic metamaterials

194 Soils are composed of subgrade soils and ground soils. There are three layers in subgrade:
 195 surface layer with a depth of 0.4 m, bottom layer with a depth of 2.3 m, and subgrade body
 196 with a depth of 2.4 m [4]. The ground consists of one layer with a depth of 15 m [17]. These
 197 soils are simulated as viscoelastic material using solid elements. The mesh of brick is used to
 198 simulate a large portion of soils, and some adaptive shapes like wedge and cylinder are used
 199 to simulate the soils near SMM.

200 The concrete inclusion of SMM is simulated using solid elements in this model. Note
 201 that infinite periodic structures do not exist in practice, therefore thirty six (6×6) inclusions
 202 are constructed to demonstrate the periodic characteristics of the SMM in the model. The

203 inclusions are simulated by solid elements. The dimensions of inclusions will be discussed in
 204 the following parts.

205 As the most efficient infinite boundary, perfectly matched layers (PML) method is used
 206 to prevent spurious wave reflections from the truncated boundary [32, 33, 34, 35, 36, 37].



207
 208 Figure 4 The 3D coupled train-track-soil model in LS-DYNA

209
 210 Table 1 Material properties of soils and SMM

Components		Density (kg/m ³)	Modulus of elasticity (MPa)	Poisson's ratio	Rayleigh damping
Subgrade [4]	Surface layer	2300	200	0.25	
	Bottom layer	1950	150	0.35	$\alpha=0$
	Subgrade body	2100	110	0.3	$\beta=0.0002$
Ground [17]	Ground soft soil	1800	20	0.3	
SMM [17]	Concrete inclusions	2500	40000	0.2	-

211

212 Figure 4 illustrates the coupled train-track-soil model in LS-DYNA. The dimension of
 213 the ground is 120 m × 130 m × 15 m. A double-track railway, which is commonly constructed

214 in China, is simulated in the model. Note that the SMM is built at the right side of the railway,
 215 while the left side of ground has the same mesh but with ground soils inside. The materials
 216 properties of the soils and SMM are shown in Table 1.

217 3.3 Numerical solution

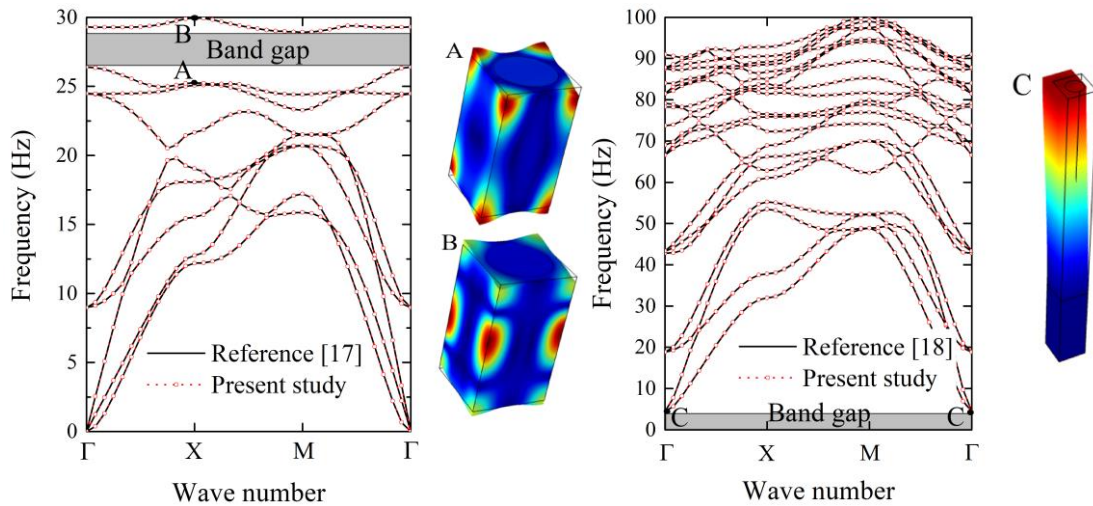
218 The vehicle is set to travel at a constant speed over the rail after the dynamic relaxation.
 219 The explicit central difference method is used to integrate the equations of motion of the
 220 coupled train-track-soil system by LS-DYNA with a time step of 1.23×10^{-5} s.

221 4. Model validation

222 The concrete and steel inclusions of the SMM are adopted to validate the proposed
 223 dispersion theory. The material properties and dimensions of the two types of inclusions are
 224 shown in table 2. The boundary conditions are set according to previous references [17, 18].

225 Table 2 Material properties and dimensions of two types of inclusions of SMM

SMM		Density (kg/m ³)	Modulus of elasticity (MPa)	Poisson's ratio	a (m)	r (m)	h (m)
Concrete inclusion [17]	Concrete	2500	40000	0.2	3	1.2	6
	Soil	1800	20	0.3			
Steel inclusion [18]	Steel	7850	200000	0.33	2	0.6	15+5 (bedrock)
	Soil	1800	153	0.3			



227

(a)

(b)

228

Figure 5 Dispersion relations and mode shapes of SMM (a) Concrete inclusion (b) Steel

229

inclusion

230

231

232

233

234

235

236

237

The dispersion relation and mode shapes of the concrete and steel inclusions of the SMM are shown in Figure 5. The concrete inclusion has a band gap of 26-29 Hz, while the steel inclusion shows a band gap of 0-4.5 Hz, indicating that the dynamic waves will be theoretically attenuated at these frequencies within band gaps. The dispersion curves obtained from this study exhibit a very good agreement with previous references [17, 18]. Also, the mode shapes are quite similar to those from references [17, 18]. Therefore, the dispersion theory proposed in this study can illustrate the theoretical dispersion characteristics of the SMM.

238

239

The 3D coupled train-track-soil interaction model has been validated in previous studies, and the validation results can be found from [4] and [5].

240

5. Ground vibration analysis

241

242

243

244

245

246

247

248

The pronounced frequency components should be mitigated in railways, and they correspond to the theoretical band gap of SMM. However, the band gaps vary with the dimensions of SMM. In order to determine the lattice constant and radius of the inclusions, the dominant frequencies of natural ground are first investigated from the coupled train-track-soil interaction model. The dimensions of the SMM are thus determined based on the pronounced frequency components of natural ground. The vibration responses from the models with and without SMM are then compared in time and frequency domain to illustrate the ground vibration mitigation effects using SMM in high-speed railways.

249

5.1 Dimensions of seismic metamaterials

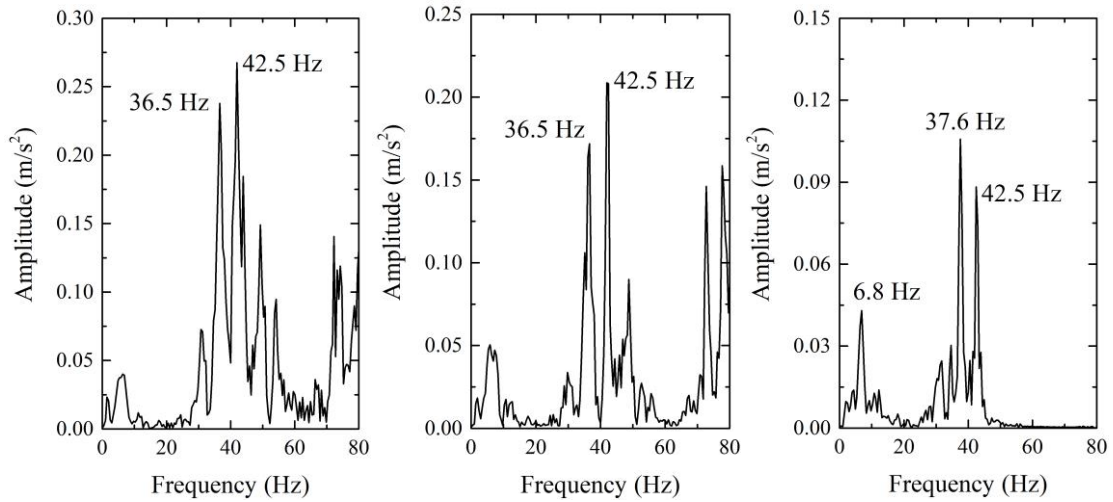
250

251

252

253

The frequency components of natural ground are obtained by applying Fast Fourier Transformation (FFT) to time history of vibration accelerations when the train travels with a speed of 380 km/h. Figure 6 illustrates the frequency distribution of railway ground without SMM.



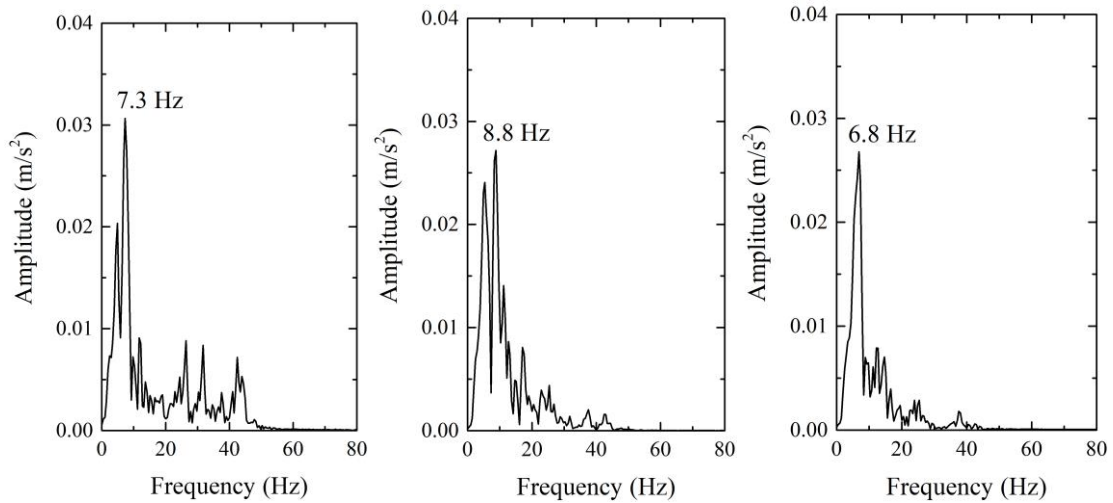
254

(a)

(b)

(c)

255



256

(d)

(e)

(f)

257

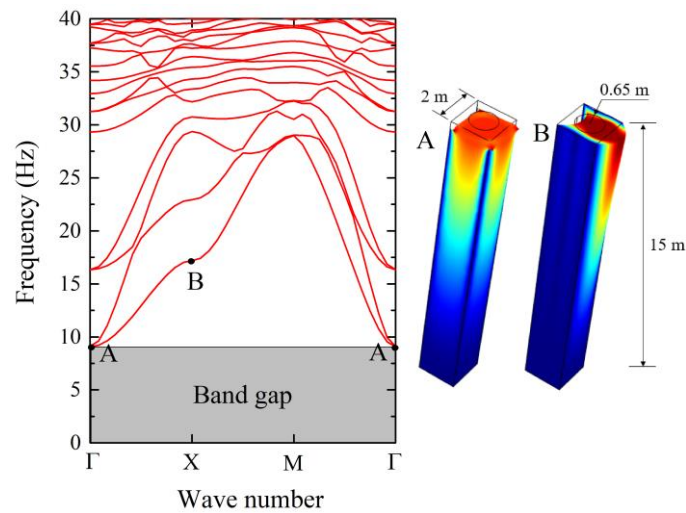
258 Figure 6 Frequency distribution of natural ground with varied lateral distances (a) 4.3 m (b)

259 11.4 m (c) 18.4 m (d) 24.4 m (e) 30 m (f) 36.4 m

260 When the soil is relatively close to the railway track (≤ 18.4 m), the pronounced
 261 frequencies are distributed in 36.5 - 42.5 Hz, as shown in Figure 6 (a), (b) and (c). It is likely
 262 that the repeated actions of wheelsets induce the component of 42.5 Hz as the theoretical
 263 frequency is $f_1 = v / l_1 = 380 / 3.6 / 2.5 = 42.2 \text{ Hz}$ (l_1 is the distance between two wheelsets).
 264 The resonance of track irregularities might induce the 36.5 Hz or 37.6 Hz. When the distance
 265 is longer than 18.4 m, the lower frequencies become dominant. The pronounced frequencies
 266 are in the range of 6.8 – 8.8 Hz, as shown in Figure 6 (d), (e) and (f). The repeated actions of
 267 bogies likely induce this frequency since the theoretical frequency is

268 $f_2 = v/l_2 = 380/3.6/17.5 = 6.03\text{Hz}$ (l_2 is the distance between two bogies). Small
269 differences between frequency components, such as 6.8 Hz and 8.8 Hz, are likely caused by
270 different mesh sizes. Note that the environmental structures and residents are normally
271 located at distances longer than 18.4 m, the attenuated frequencies should be lower than 9 Hz
272 in this case.

273 The concrete inclusions are adopted in high-speed railways in this study. The depth of the
274 SMM is 15 m to simulate the deep thickness according to [17]. Based on the characteristics of
275 concrete inclusions from [17], the SMM exhibits a theoretical band gap with 0 - 9.1 Hz when
276 the lattice constant is 2 m and radius of inclusions is 0.65 m, as shown in Figure 7. Therefore,
277 the SMM with the selected dimensions can theoretically attenuate the dynamic vibrations
278 with frequencies lower than 9.1 Hz, which is in line with the target frequencies obtained from
279 the coupled train-track-soil interaction model. Also, the mode shapes at Point A and Point B
280 exhibit a shear-like mode [18], indicating that the SMM can attenuate shear waves in railways.
281 In short, the SMM with lattice constant of 2 m and radius of 0.65 m and depth of 15 m is
282 adopted in the coupled train-track-soil interaction model to investigate the ground vibration
283 mitigation effect in high-speed railways.

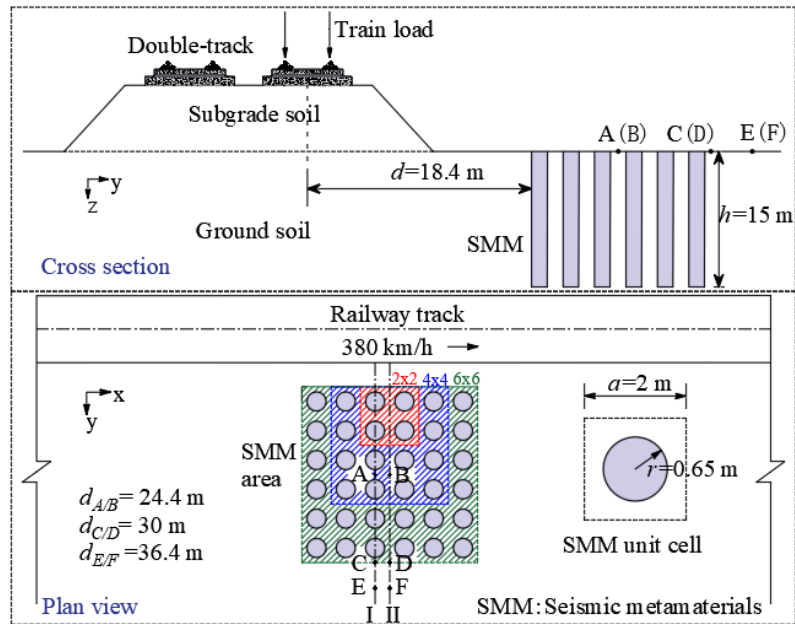


284

285

Figure 7 Dispersion relation and mode shapes of the SMM adopted in railways

286 **5.2 Mitigation effect using seismic metamaterials**

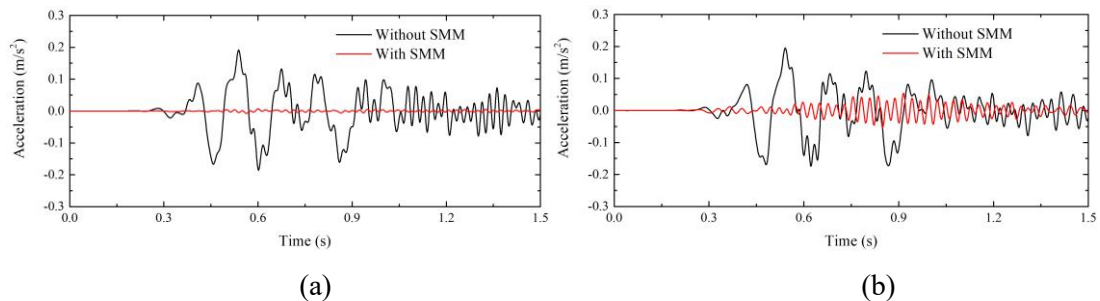


287

288 **Figure 8 Distribution of the SMM and monitor points in railways**

289 The SMM with 36 (6×6) concrete inclusions is adopted in the railway ground, as
 290 illustrated in Figure 8. The initial distance (d) between the front edge of SMM and the center
 291 line of the right track is 18.4 m. The lateral distance along with two lines (Line I and Line II)
 292 are chosen as monitoring locations in this railway. Six points (Point A, B, C, D, E, and F) with
 293 different lateral distances are also selected as key points. The vibration responses from these
 294 monitoring locations are compared in both time and frequency domains.

295 **5.2.1 Time domain analysis**



296

297

(a)

(b)

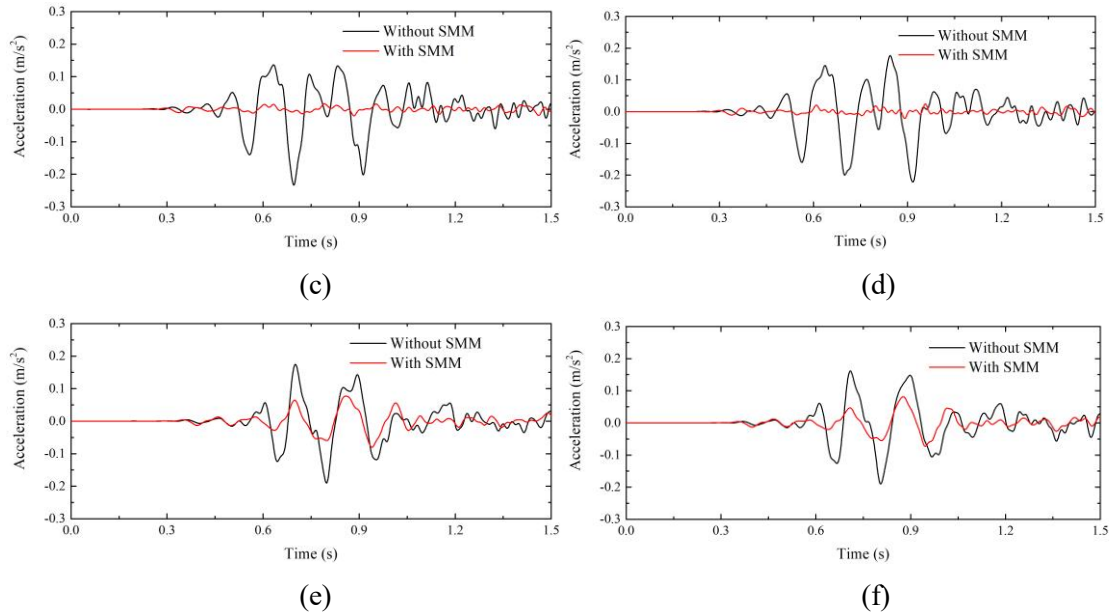


Figure 9 Time history of vibration accelerations (a) Point A (b) Point B (c) Point C (d) Point D (e) Point E (f) Point F

Figure 9 shows the time history curves of the vibration accelerations at six key points in this railway. The SMM exhibits a significant vibration mitigation effect as the amplitudes of vibration accelerations with SMM are much lower than those without SMM. The attenuation effect is quite similar at 24.4 m (A and B) and 30 m (C and D). But the mitigation effect weakens at 36.4 m since Point E and F are located behind the SMM area.

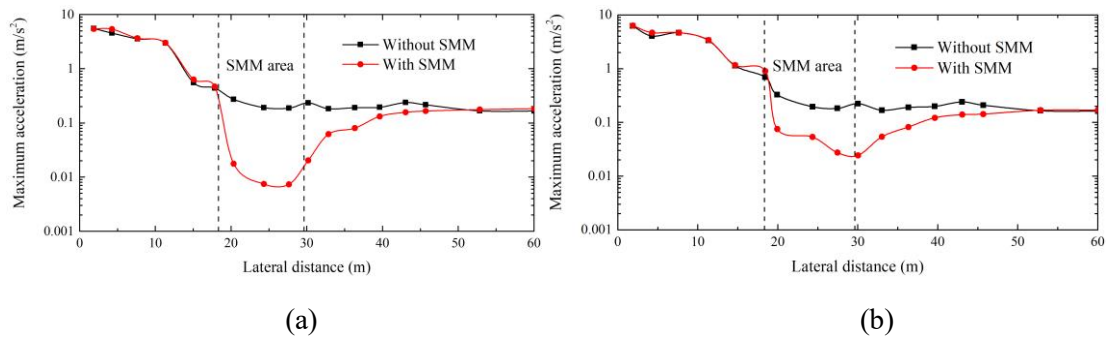
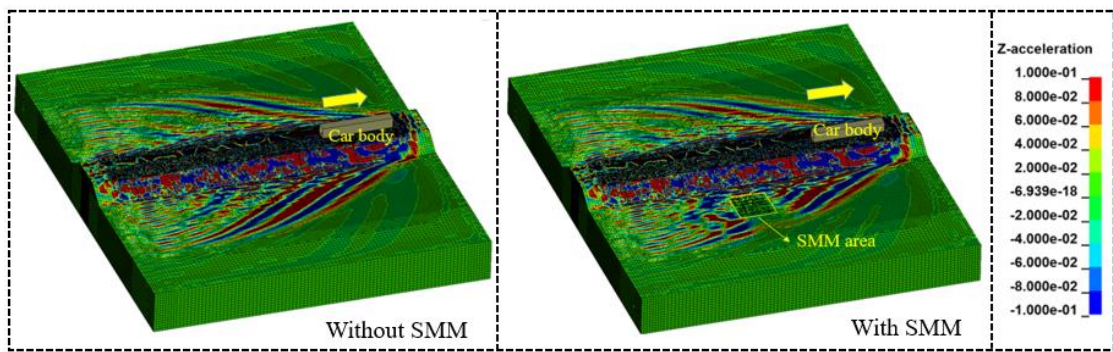


Figure 10 Maximum acceleration with lateral distance (a) Line I (b) Line II

The maximum accelerations along with Line I and Line II are shown in Figure 10. When the distance is shorter than 18.4 m, which is the front edge of SMM area, the maximum accelerations with and without SMM exhibit no evident differences. However, when the dynamic waves approach the SMM area, the SMM exhibits a significant vibration mitigation effect. The maximum acceleration achieves a maximum reduction of 96% from 0.19 m/s^2 to 0.007 m/s^2 in Line I, and 91% from 0.22 m/s^2 to 0.02 m/s^2 in Line II. Globally, the reduction

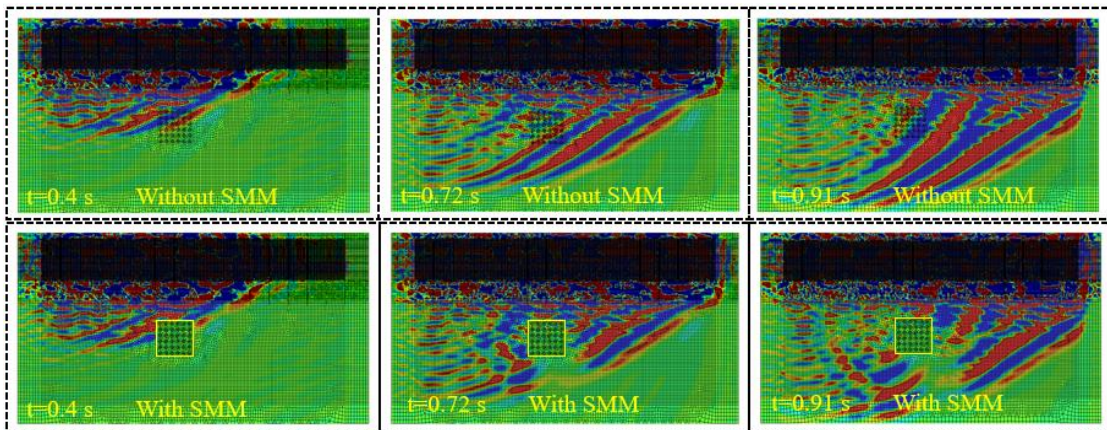
318 effect along with Line I is better than that along with Line II. The significant vibration
 319 mitigation effect is mainly induced by the higher modulus and density that SMM possesses.
 320 When the distance is longer than the back edge of SMM area, the SMM can still attenuate the
 321 vibration accelerations. And the maximum accelerations converge to the same magnitude
 322 when the distance is longer than 50 m. It is noted that when the SMM is adopted in the
 323 railway, the maximum acceleration at 18.4 m is a little bit higher than that without SMM. It is
 324 likely that the dynamic waves reflect when they approach the barriers, resulting in higher
 325 ground vibration response at the front edge of SMM area.



326

327

(a)



328

329

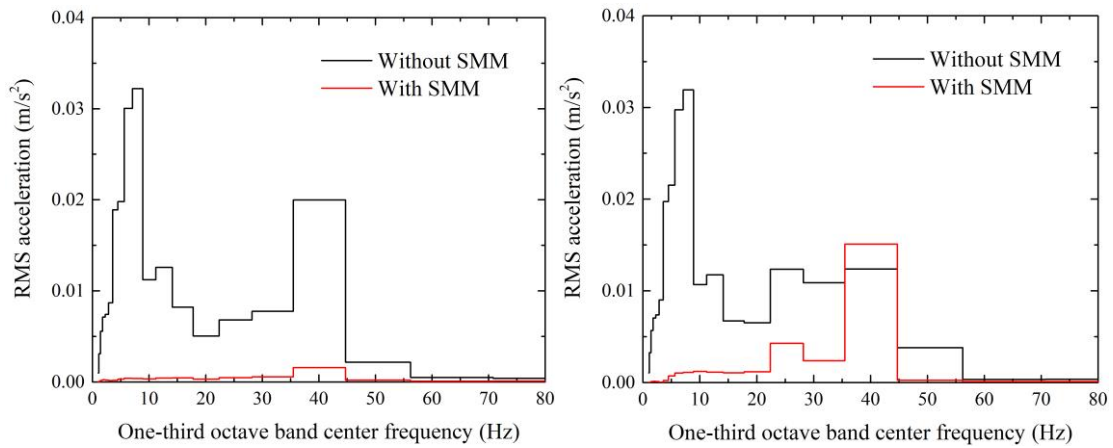
(b)

330 Figure 11 Contours of the ground vibration acceleration (a) 3D view (b) plan view

331 Figure 11 illustrates the contours of the ground vibration acceleration with two cases:
 332 with and without SMM. Note that the acceleration values are set between -0.1 m/s^2 and 0.1
 333 m/s^2 in order to present a clear propagation path of dynamic waves. The Mach cone
 334 phenomenon, which is analogous to a boat moving through the water, can be observed from
 335 the 3D view in both cases. But the SMM affects the propagations of dynamic waves, as

336 shown in Figure 11 (a). Figure 11 (b) illustrates the distribution of waves varies with time.
337 When the ground is natural, the dynamic waves can propagate continuously all the time.
338 However, when the SMM is adopted, the dynamic waves change their propagation paths due
339 to the barriers. The accelerations in the SMM area and at the right-back of SMM area exhibit
340 noticeable vibration shielding effects.

341 5.2.2 Frequency domain analysis

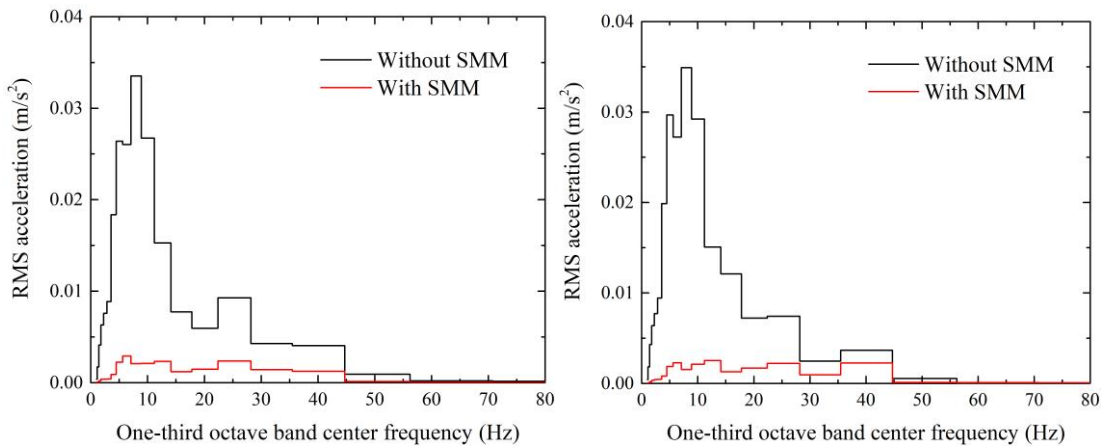


342

343

(a)

(b)

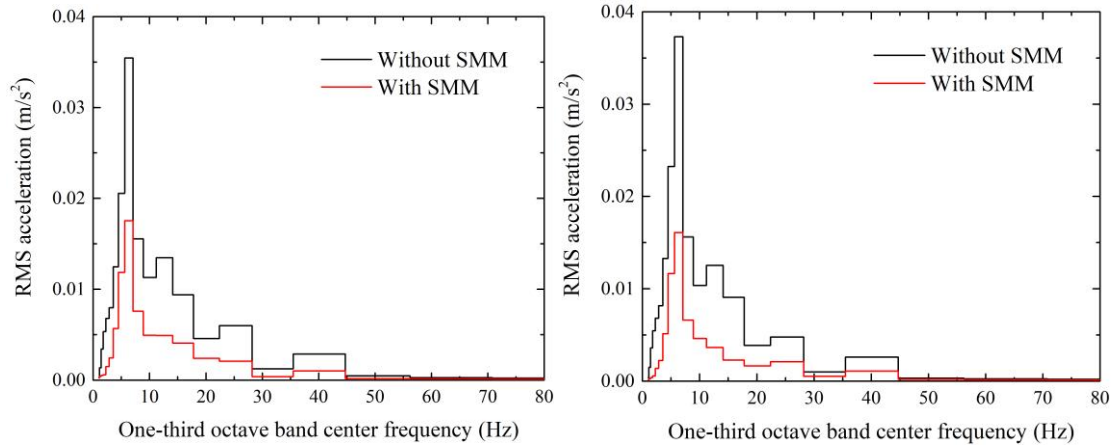


344

345

(c)

(d)



(e)

(f)

Figure 12 One-third octave band RMS spectrum of the acceleration level of ground (a) Point A (b) Point B (c) Point C (d) Point D (e) Point E (d) Point F

The root mean square (RMS) acceleration is an important indicator to evaluate the vibration level. The time histories of the ground vibration acceleration at a one-third octave band are obtained by conducting the filter processing to the frequency components. And the one-third octave band RMS spectrum can be calculated as follows:

$$a_{rms} = \sqrt{\lim_{N_s \rightarrow \infty} \frac{1}{N_s} \sum_{k=0}^{N_s} [a_w(k)]^2} \quad (8)$$

where $a_w(k)$ is the discrete-time history of acceleration at a one-third octave band, and N_s is the sampling number.

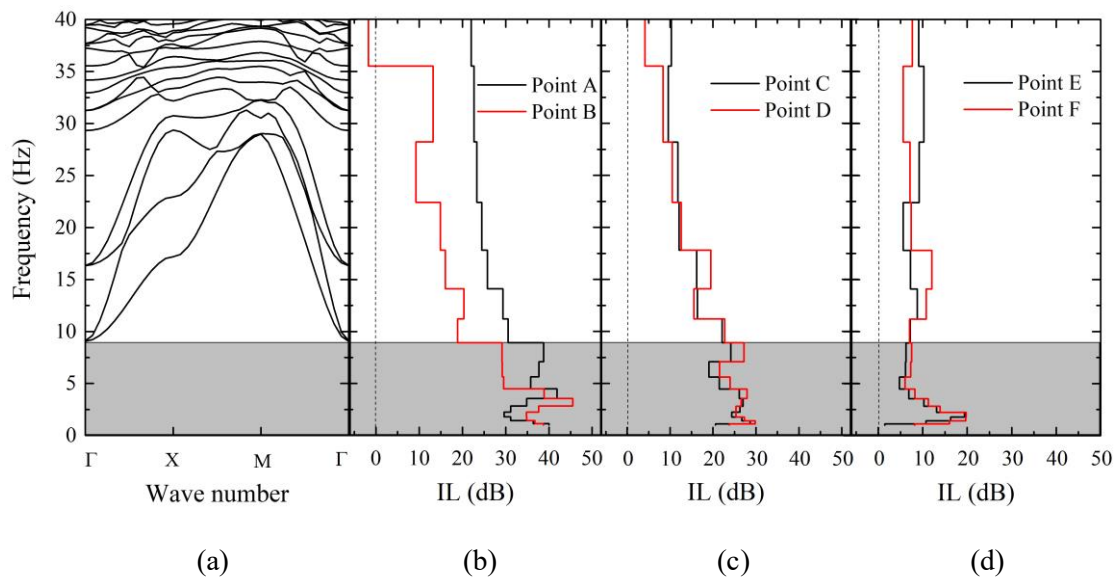
The one-third octave band RMS spectrum at six key points are shown in Figure 12. The SMM exhibits excellent ground vibration mitigation effects in frequency domain. When the ground is natural, the pronounced frequency components are around 8 Hz and 40 Hz at Point A and B, but the frequency component of 8 Hz is significantly reduced when the SMM is adopted, as shown in Figure 12 (a) and (b). A similar reduction effect by using SMM can be observed for Point C, D, E and F. Since the theoretical band gap is 0-9.1 Hz, the dispersion relation predicts the attenuation frequency bands quite well. It is also noted that the reduction components are not only the pronounced component of 8 Hz but also the frequencies with a relatively large band (around 0-45 Hz), indicating that SMM could have a better mitigation effect in reality than theoretical predictions from dispersion analysis.

To quantify how much the acceleration level has been reduced due to the SMM in the

368 one-third octave band RMS spectrum, the insertion loss (IL) from the ratio of the RMS
 369 acceleration of the ground without and with SMM is calculated as follows:

$$370 \quad IL = 20 \cdot \lg \frac{a_{\text{without}}}{a_{\text{with}}} \quad (9)$$

371 where a_{without} is the RMS acceleration of the ground without SMM, and a_{with} denotes the
 372 RMS acceleration of the ground with SMM. Positive values indicate a significant reduction of
 373 vibration level, while negative values correspond to an inverse amplification effect using
 374 SMM.



375
 376 (a) (b) (c) (d)
 377 Figure 13 Insertion loss (a) Theoretical band gap (b) IL at Point A and B (c) IL at Point C and
 378 D (d) IL at Point E and F

379 Figure 13 illustrates the IL at six key points when they are compared with the theoretical
 380 band gap. The SMM can reduce the vibration level with an IL of around 45 dB at 24.4 m
 381 (Point A and B). The maximum IL is 30 dB and 20 dB at 30 m (Point C and D) and 36.4 m
 382 (Point E and F), respectively. Therefore, the maximum mitigation effect reduces with the
 383 three distances. The IL shows its maximum values at frequencies of 0-9.1 Hz, which
 384 corresponds to the theoretical band gap. In addition, the SMM also globally exhibits good
 385 vibration mitigation effect when frequencies are lower than 40 Hz.

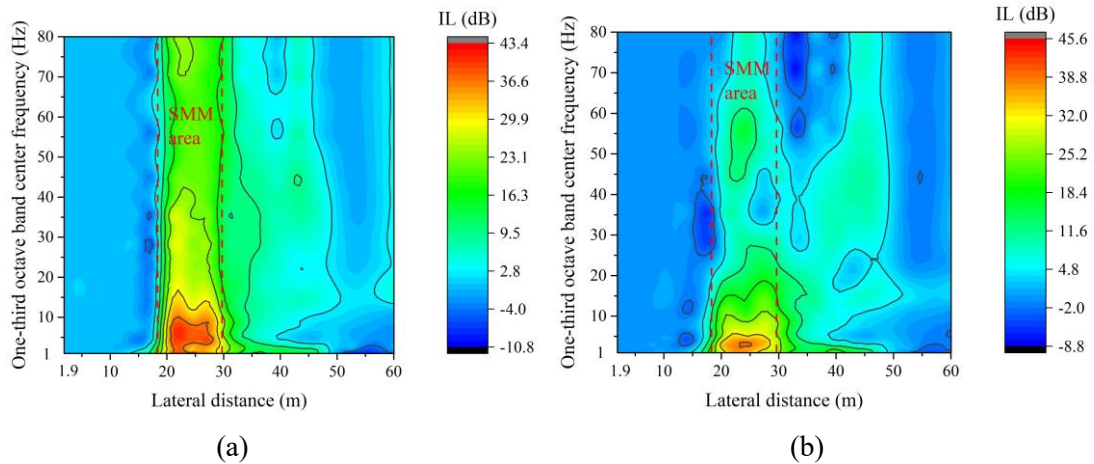


Figure 14 Insertion loss (a) Line I (b) Line II

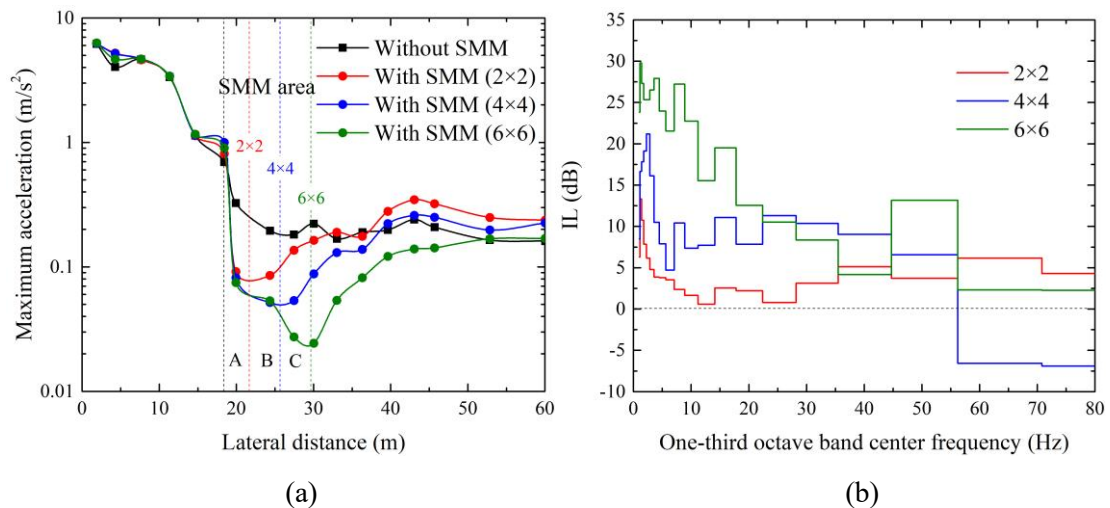
The IL along with two lines are shown in Figure 14. The maximum IL occurs in the SMM area at frequencies lower than 9 Hz, indicating the SMM performs a significant vibration attenuation effect. The two lines show a similar phenomenon referring to the IL, but the maximum IL has small differences (43.3 dB for Line I, and 45.6 dB for Line II).

6. Parametric studies

In order to obtain a comprehensive knowledge of the ground vibration mitigation using SMM in railways, the number of inclusions, the initial distances of the SMM, and the train speeds are changed to investigate their influences on the attenuation effects.

6.1 Number of inclusions

The number of inclusions is chosen as 2×2 , 4×4 , and 6×6 . The distribution of different numbers of inclusions can be seen from Figure 8. Figure 15 shows the ground vibration mitigation results under three cases.



401
402

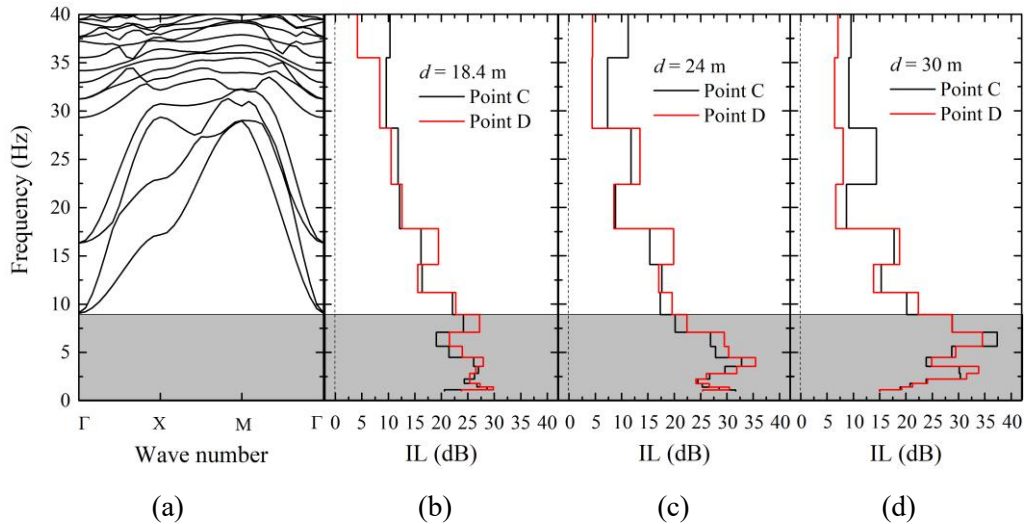
403 Figure 15 Ground vibration responses with different numbers of inclusions (a) Maximum
404 acceleration along with Line II (b) Insertion loss at Point D

405 As shown in Figure 15 (a), the region A represents that the positions are located in SMM
406 area for all three cases (2×2, 4×4, and 6×6, red square in Figure 8). The positions in region B
407 are in SMM area for two cases (4×4, and 6×6, blue square in Figure 8), and points in region C
408 are only in SMM area with 6×6 inclusions (Green square in Figure 8). In all three cases, the
409 mitigation effect appears when the dynamic waves approach the SMM area. In region A, the
410 values of attenuated accelerations are quite similar for three cases. In region B, the
411 accelerations in the case of 4×4 inclusions are lower than those of 2×2 inclusions, but they are
412 identical with those of 6×6 inclusions. In region C, the case of 6×6 inclusions exhibits the best
413 mitigation effect. Therefore, no matter the number of inclusions, the SMM has similar
414 mitigation acceleration values as long as the locations are within the area of periodic barriers.
415 When the distance overtakes the back edge of the SMM area, the accelerations are recovered,
416 and the values can be higher than those of natural ground.

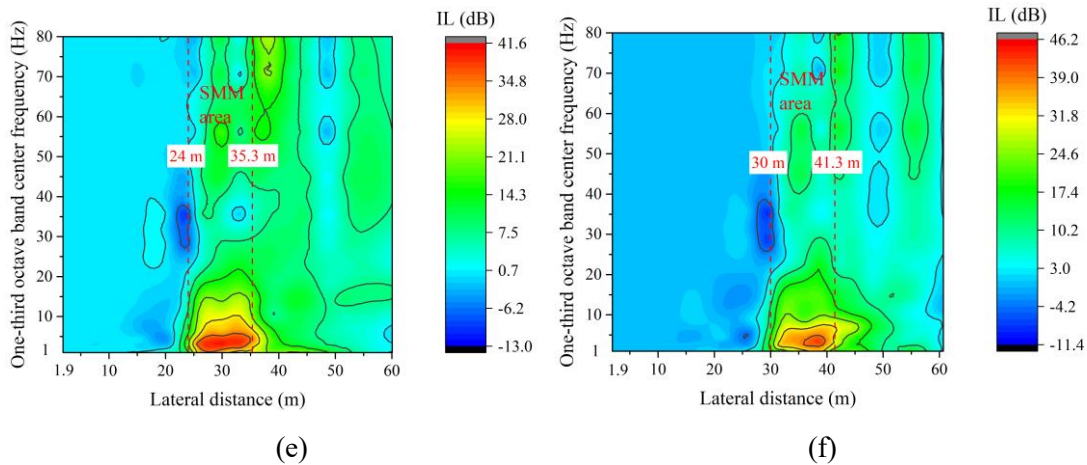
417 The IL with cases of 2×2, 4×4, and 6×6 inclusions is shown in Figure 15 (b). The case of
418 6×6 inclusions has maximum IL with 30 dB, while the case of 4×4 inclusions exhibits 23 dB,
419 and the 2×2 inclusions can reduce the vibration level with 13 dB. Therefore, when
420 frequencies are lower than 45 Hz, the mitigation of ground vibration level is significant with
421 increasing the number of inclusions. Also, the maximum values of IL occur at frequencies
422 lower than 9 Hz for three cases, corresponding to the theoretical dispersion prediction. It is
423 also noted that the case of 4×4 inclusions exhibits negative values of IL when the frequencies

424 are higher than 55 Hz, indicating that the vibration level can be amplified due to the
 425 propagations of dynamic waves behind the SMM area.

426 **6.2 Initial distance**



427
 428



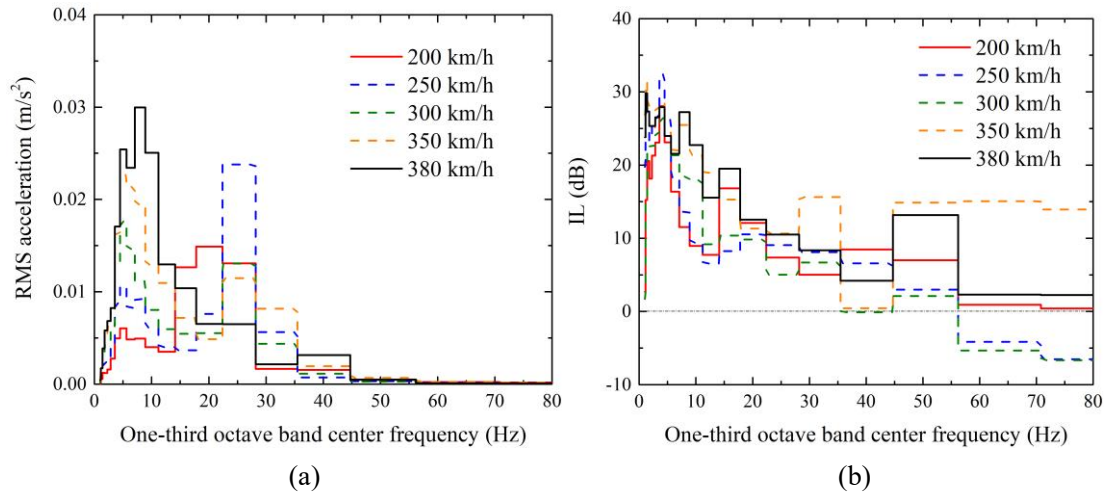
429
 430

431 Figure 16 Insertion loss with different initial distances (a) theoretical band gap (b) IL at two
 432 points when $d=18.4$ m (c) IL at two points when $d=24$ m (d) IL at two points when $d=30$ m
 433 (e) IL distribution with Line II when $d=24$ m (f) IL distribution with Line II when $d=30$ m

434 The initial distance (d , as shown in Figure 8) between the front edge of the SMM and the
 435 center line of the track is varied for 18.4 m, 24 m and 30 m. Figure 16 shows the IL with three
 436 cases. Note that Point C and D are relative positions to the SMM area in Figure 16 (b), (c) and
 437 (d). When $d=18.4$ m, $d_{C/D}=30$ m; When $d=24$ m, $d_{C/D}=35.6$ m; and when $d=30$ m, $d_{C/D}=$
 438 41.6 m. The IL at Point C and D exhibit a similar tendency for three cases. Although the
 439 maximum values of IL have some differences, they occur at the frequencies of 0-9.1 Hz. The

440 IL distribution can also reflect the SMM locations since the maximum IL appears in SMM
441 area, as shown in Figure 16 (e) and (f). Therefore, the initial distance exhibits an insignificant
442 influence on the ground vibration mitigation effect using SMM.

443 6.3 Train speed



446 Figure 17 Ground vibration responses with varied train speeds (a) One-third octave band
447 RMS spectrum of ground without SMM at Point D (b) IL at Point D

448 The train speed is changed from 200 km/h to 380 km/h. Since the frequency components
449 of ground can change with train speed, the one-third octave band RMS spectrum of natural
450 ground is first obtained with five cases of train speeds, as shown in Figure 17 (a). When the
451 train speed is relatively lower (200 km/h and 250 km/h), the pronounced frequencies are
452 distributed in 20-30 Hz. When the train speed is higher (≥ 300 km/h), the frequency
453 components within 9 Hz are more evident. Figure 17 (b) shows the corresponding IL with
454 different train speeds. Although the significant frequency components change with train
455 speeds, the mitigation of ground vibration level is still pronounced within frequencies lower
456 than 9 Hz since the band gap is one of the inherent characteristics of the SMM. It is noted that
457 the distribution of IL is scattered with different train speeds when the frequencies are higher
458 than 40 Hz, but it is insignificant since the RMS accelerations are quite low at these
459 frequencies.

460 7. Conclusions

461 As an innovative vibration mitigation solution, seismic metamaterial (SMM) has received
462 increasing attention as it can theoretically shield dynamic waves in certain frequency bands.
463 However, the application of the SMM in railways is recent, and the related research is
464 ongoing, so the mitigation effects by SMM in railway-induced ground vibrations are still
465 unknown. This study is thus the world's first to investigate the ground vibration mitigation
466 using SMM-based barriers in high-speed railways. The dispersion theory is proposed to
467 obtain the theoretical band gaps of the SMM. In order to investigate the influence of SMM on
468 the ground vibrations, a 3D coupled train-track-soil model is developed based on the
469 multi-body simulation principle, finite element theory and perfectly matched layers method
470 using LS-DYNA. The proposed models were validated by comparing the results with
471 previous works. Based on the ground vibration responses from the models with and without
472 SMM, the following conclusions can be drawn:

473 (a) The pronounced frequency components should be attenuated in railways, and they
474 correspond to the theoretical band gap of SMM. Although the dominant frequencies of natural
475 ground vary with the distance from the railway track, they are lower than 9 Hz at longer
476 distances in this study. The SMM, which is adopted in this railway, possesses a band gap with
477 0 - 9.1 Hz.

478 (b) In time domain, the SMM performs an excellent vibration mitigation effect. The
479 mitigation of acceleration occurs both in and behind the SMM area. The accelerations reduce
480 by a maximum of 96%. Also, the SMM interferes with the propagation paths of dynamic
481 waves and attenuates the vibration accelerations.

482 (c) In frequency domain, the most significant vibration mitigation components in
483 railways correspond to the theoretical dispersion predictions, which is lower than 9 Hz.
484 However, the SMM globally exhibits a better mitigation effect in railways. The SMM can
485 significantly reduce the ground vibration level since the maximum insertion loss is higher
486 than 40 dB.

487 (d) The number of inclusions can increase the mitigation effect of SMM, while the initial
488 distance of SMM exhibits an insignificant impact on ground vibrations. In addition, the train

489 speed can arouse different pronounced frequency components, but the mitigation components
490 are still determined based on the dispersion relations. Therefore, when the SMM is adopted in
491 railways, the number of inclusions and train speed should be considered in practice.

492 It is also noted that this study aims to create new contribution towards a better
493 understanding into the mitigation effects by SMM for railway-induced ground vibrations.
494 This simulation can reflect the vibration mitigation effect using SMM to a certain extent.
495 Further experimental studies are recommended to be investigated in the future before the
496 SMM is adopted in railways in practice.

497 **Acknowledgments**

498 This research was supported by the Key Research Development Program of China
499 (No.2016YFC0802203-2, No.2016YFC0802203-3). The authors sincerely thank European
500 Commission for H2020-MSCA-RISE Project No. 691135 “RISEN: Rail Infrastructure
501 Systems Engineering Network,” which enables a global research network that tackles the
502 grand challenge in railway infrastructure resilience and advanced sensing under extreme
503 conditions (www.risen2rail.eu) [38].

504 **References**

- 505 [1] Connolly DP, Marecki GP, Kouroussis G, Thalassinakis I, Woodward PK. The growth of railway
506 ground vibration problems - A review. *Science of the Total Environment*. 2016;568:1276-82.
- 507 [2] Remennikov AM, Kaewunruen S. A review of loading conditions for railway track structures due to
508 train and track vertical interaction. *Struct Control Health Monit*. 2008;15(2):207-34.
- 509 [3] Zhai WM, Han ZL, Chen ZW, Ling L, Zhu SY. Train-track-bridge dynamic interaction: a
510 state-of-the-art review. *Vehicle System Dynamics*. 2019;57(7):984-1027.
- 511 [4] Li T, Su Q, Kaewunruen S. Influences of piles on the ground vibration considering the
512 train-track-soil dynamic interactions. *Computers and Geotechnics*. 2020;120:12.
- 513 [5] Li T, Su Q, Kaewunruen S. Saturated Ground Vibration Analysis Based on a Three-Dimensional
514 Coupled Train-Track-Soil Interaction Model. *Appl Sci-Basel*. 2019;9(23):18.
- 515 [6] Li ZG, Wu TX. On vehicle/track impact at connection between a floating slab and ballasted track
516 and floating slab track's effectiveness of force isolation. *Vehicle System Dynamics*. 2009;47(5):513-31.
- 517 [7] Sol-Sanchez M, Moreno-Navarro F, Rubio-Gamez MC. The use of elastic elements in railway
518 tracks: A state of the art review. *Construction and Building Materials*. 2015;75:293-305.
- 519 [8] Connolly D, Giannopoulos A, Fan W, Woodward PK, Forde MC. Optimising low acoustic
520 impedance back-fill material wave barrier dimensions to shield structures from ground borne high
521 speed rail vibrations. *Construction and Building Materials*. 2013;44:557-64.

522 [9] Thompson DJ, Jiang J, Toward MGR, Hussein MFM, Ntotsios E, Dijckmans A, et al. Reducing
523 railway-induced ground-borne vibration by using open trenches and soft-filled barriers. *Soil Dynamics
524 and Earthquake Engineering*. 2016;88:45-59.

525 [10] Pu XB, Shi ZF. Surface-wave attenuation by periodic pile barriers in layered soils. *Construction
526 and Building Materials*. 2018;180:177-87.

527 [11] Colombi A, Roux P, Guenneau S, Gueguen P, Craster RV. Forests as a natural seismic
528 metamaterial: Rayleigh wave bandgaps induced by local resonances. *Sci Rep*. 2016;6:7.

529 [12] Muhammad, Lim CW, Reddy JN. Built-up structural steel sections as seismic metamaterials for
530 surface wave attenuation with low frequency wide bandgap in layered soil medium. *Engineering
531 Structures*. 2019;188:440-51.

532 [13] An XY, Fan HL, Zhang CZ. Elastic wave and vibration bandgaps in two-dimensional acoustic
533 metamaterials with resonators and disorders. *Wave Motion*. 2018;80:69-81.

534 [14] Brule S, Enoch S, Guenneau S. Emergence of seismic metamaterials: Current state and future
535 perspectives. *Phys Lett A*. 2020;384(1):11.

536 [15] Peng H, Pai PF. Acoustic metamaterial plates for elastic wave absorption and structural vibration
537 suppression. *Int J Mech Sci*. 2014;89:350-61.

538 [16] Kaewunruen S, Martin V. Life Cycle Assessment of Railway Ground-Borne Noise and Vibration
539 Mitigation Methods Using Geosynthetics, Metamaterials and Ground Improvement. *Sustainability*.
540 2018;10(10):21.

541 [17] Chen YY, Qian F, Scarpa F, Zuo L, Zhuang XY. Harnessing multi-layered soil to design seismic
542 metamaterials with ultralow frequency band gaps. *Mater Des*. 2019;175:8.

543 [18] Achaoui Y, Antonakakis T, Brule S, Craster RV, Enoch S, Guenneau S. Clamped seismic
544 metamaterials: ultra-low frequency stop bands. *New J Phys*. 2017;19:13.

545 [19] Huang JK, Liu W, Shi ZF. Surface-wave attenuation zone of layered periodic structures and
546 feasible application in ground vibration reduction. *Construction and Building Materials*.
547 2017;141:1-11.

548 [20] Huang JK, Shi ZF. Attenuation zones of periodic pile barriers and its application in vibration
549 reduction for plane waves. *Journal of Sound and Vibration*. 2013;332(19):4423-39.

550 [21] Krodel S, Thome N, Daraio C. Wide band-gap seismic metastructures. *Extreme Mech Lett*.
551 2015;4:111-7.

552 [22] Ungureanu B, Achaoui Y, Enoch S, Brule S, Guenneau S. Auxetic-like metamaterials as novel
553 earthquake protections. *EPJ Appl Metamaterials*. 2016;2:8.

554 [23] Brule S, Javelaud EH, Enoch S, Guenneau S. Experiments on Seismic Metamaterials: Molding
555 Surface Waves. *Phys Rev Lett*. 2014;112(13):5.

556 [24] Brule S, Javelaud EH, Enoch S, Guenneau S. Flat lens effect on seismic waves propagation in the
557 subsoil. *Sci Rep*. 2017;7:9.

558 [25] Miniaci M, Krushynska A, Bosia F, Pugno NM. Large scale mechanical metamaterials as seismic
559 shields. *New J Phys*. 2016;18:14.

560 [26] Meng LK, Cheng ZB, Shi ZF. Vibration mitigation in saturated soil by periodic pile barriers.
561 *Computers and Geotechnics*. 2020;117:9.

562 [27] Thompson DJ, Kouroussis G, Ntotsios E. Modelling, simulation and evaluation of ground
563 vibration caused by rail vehicles. *Vehicle System Dynamics*. 2019;57(7):936-83.

564 [28] Shi ZF, Chen ZB; Xiang HJ. *Periodic structures: Theory and Applications to seismic isolation and
565 vibration reduction*. Beijing. 2017.

566 [29] Pu XB, Shi ZF. A novel method for identifying surface waves in periodic structures. *Soil*
567 *Dynamics and Earthquake Engineering*. 2017;98:67-71.

568 [30] Wang MZ, Cai CB, Zhu SY, Zhai WM. Experimental study on dynamic performance of typical
569 nonballasted track systems using a full-scale test rig. *Proc Inst Mech Eng Part F-J Rail Rapid Transit*.
570 2017;231(4):470-81.

571 [31] Lei XY, Wang J. Dynamic analysis of the train and slab track coupling system with finite elements
572 in a moving frame of reference. *Journal of Vibration and Control*. 2014;20(9):1301-17.

573 [32] Basu U. Explicit finite element perfectly matched layer for transient three-dimensional elastic
574 waves. *International Journal for Numerical Methods in Engineering*. 2009;77(2):151-76.

575 [33] Wang J, Jin X, Cao Y. High-speed maglev train-guideway-tunnel-soil modelling of ground
576 vibration. *Proc Inst Mech Eng Part F-J Rail Rapid Transit*. 2012;226(F3):331-44.

577 [34] Kouroussis, G., Connolly, D. P., Verlinden, O. Railway-induced ground vibrations—a review of
578 vehicle effects. *International Journal of Rail Transportation*, 2014, 2(2), 69-110.

579 [35] Kaewunruen, S., Remennikov, A.M. Current state of practice in railway track vibration isolation:
580 an Australian overview, *Australian Journal of Civil Engineering*, 2016, 14:1, 63-71, DOI:
581 10.1080/14488353.2015.1116364

582 [36] Ngamkhanong, C., Kaewunruen, S., The effect of ground borne vibrations from high speed train
583 on overhead line equipment (OHLE) structure considering soil-structure interaction, *Science of The*
584 *Total Environment*, 2018, 627, 934-941.

585 [37] Ngamkhanong C, Kaewunruen S and Baniotopoulos C (2018) Far-Field Earthquake Responses of
586 Overhead Line Equipment (OHLE) Structure Considering Soil-Structure Interaction. *Front. Built*
587 *Environ.* 4:35. doi: 10.3389/fbuil.2018.00035

588 [38] Kaewunruen S, Sussman JM and Matsumoto A (2016) Grand Challenges in Transportation and
589 Transit Systems. *Front. Built Environ.* 2:4. doi: 10.3389/fbuil.2016.00004

590